Title	The numerical steepest descent path method for calculating physical optics integrals on smooth conducting quadratic surfaces
Author(s)	Wu, Y; Jiang, L; Sha, W; Chew, WC
Citation	IEEE Transactions on Antennas and Propagation, 2013, v. 61 n. 8, p. 4183-4193
Issued Date	2013
URL	http://hdl.handle.net/10722/185847
Rights	IEEE Transactions on Antennas and Propagation. Copyright © IEEE.

The Numerical Steepest Descent Path Method for Calculating Physical Optics Integrals on Smooth Conducting Quadratic Surfaces

Yu Mao Wu, Li Jun Jiang, *Senior Member, IEEE*, Wei E. I. Sha, *Member, IEEE*, and Weng Cho Chew, *Fellow, IEEE*

***Abstract*—In this paper, we use the numerical steepest descent path (NSDP) method to analyze the highly oscillatory physical optics (PO) integral on smooth conducting parabolic surfaces, including both monostatic and bistatic cases. Quadratic variations of the amplitude and phase functions are used to approximate the integrand of PO integral. Then the surface PO integral is reduced into several highly oscillatory line integrals. By invoking the NSDP method, these highly oscillatory PO line integrals are defined on the corresponding NSDPs. Furthermore, the critical point contributions for the PO integral are exactly extracted and represented based on the NSDPs. The proposed NSDP method for calculating the PO integral on the smooth conducting surfaces is frequency-independent and error-controllable. Compared with the traditional asymptotic expansion approach, the NSDP method significantly improves the PO integral accuracy by around two digits when the working wave frequencies are not extremely large. Numerical results are given to validate the NSDP method.**

***Index Terms*—Contribution points, highly oscillatory integral, numerical steepest descent path, physical optics (PO).**

I. Introduction

In computational electromagnetics (CEM) community, analysis of the scattered electromagnetic (EM) fields by the electrically large perfect conducting object [1], [3]–[5] is an important and challenging problem. As we know, the method of moments (MOM) [2] provides a traditional full wave approach to calculate the scattered EM fields. However, the computational effort increases as fast as $O(N^2)$, and the number of discretized meshes for the considered object N is proportional to the square of the product of the working frequency k and the size of the object d. When the electrical size of the considered objects is on the order of tens to hundreds of the working wavelength λ, that is, kd is large enough, the physical optics (PO) approximation [6]–[9] is served as an efficient approach for analyzing the scattered EM fields. Early in 1913, Macdonald [7] introduced the PO approximation concept by approximating the induced current on the surface of the simulated object. The surface PO induced current [6]–[9] is approximated by doing the local tangent plane approximation, that is, the integration small surface patch dS along the electrically large object is assumed to be locally flat and smooth under the external high frequency condition. In this sense, for the incident high frequency EM waves on the electrically large real-world objects, the PO approximation [7]–[18] has revealed itself as an efficient way to calculate the scattered field.

The scattered field generated by the surface PO induced current can be described as a highly oscillatory surface integral [1], [17]. The traditional method for calculating the PO type integral, such as the Gaussian quadrature rule [33], causes the computational effort to increase vastly as the working frequency k goes high. Hence, the challenge on developing efficient numerical methods to calculate the PO integral has attracted great interests from both engineers and mathematicians in the past several decades [10]–[32]. The traditional asymptotic expansion approximation (ASP) [1], [17] for analyzing the highly oscillatory PO integral offers a frequency-independent approach. The surface PO integrals on the considered objects are split into the contributions of critical points, including the stationary phase points (SPPs), the boundary resonance, and vertex points. Also, analysis of the critical point contributions by the ASP method [17] provides the physical insights on the high frequency wave propagation. However, the ASP method usually produces the PO integral results with limited accuracy, especially when the working frequency k is not large enough. Also, mathematicians have extensively studied the challenging PO type oscillatory integrals [22]–[27]. By making use of the ASP, efficient Filon-type and Levin-type numerical quadratures [25] are developed. Meanwhile, mathematical error analysis on these PO type oscillatory integrals was studied in [22], [25].

The integrand of the highly oscillatory PO type integral includes the slowly varying amplitude part, and the highly oscillatory part—the exponent of the phase function. Hence, approximation of the PO integrand provides a possible way to derive the closed-form formulas for the PO type integral. In [11], the PO integral on the biquadratic surface with quadratic phase was considered. Then, the closed-form formula for the PO kernel on one-parameter curve exist, while a closed-form solution to this PO kernel on the two-parameters surface does not exist. In

Manuscript received July 24, 2012; revised January 02, 2013; accepted February 11, 2013. Date of publication April 24, 2013; date of current version July 31, 2013.

Y. M. Wu is with the Department of Electrical and Electronic Engineering, The University of Hong Kong, China and also with the Department of Electrical and Computer Engineering, University of Illinois at Urbana-Champaign, Urbana, IL 61801 USA (e-mail: ymwu@eee.hku.hk).

L. J. Jiang and W. E. I. Sha are with the Department of Electrical and Electronic Engineering, The University of Hong Kong, China (e-mail: jianglj@hku.hk; wsha@eee.hku.hk).

W. C. Chew is with Department of Electrical and Computer Engineering, University of Illinois at Urbana-Champaign, Urbana, IL 61801 USA, and also on part-time appointment with The University of Hong Kong, China (e-mail: w-chew@uiuc.edu).

Color versions of one or more of the figures in this paper are available online at http://ieeexplore.ieee.org.

Digital Object Identifier 10.1109/TAP.2013.2259788

this manner, a quadrature technique for evaluating PO scattering was developed in terms of an extension of the so-called Filon quadrature. Based on the assumption that the amplitude and phase functions vary linearly, the surface PO type integral can be analytically simplified into several line integrals [28]–[30]. Then the closed form formulas were derived on the flat polygon patches. However, the linear function used to approximate the phase term in the PO integrand cannot capture the SPP and resonance points contributions of the PO integral. In this sense, the quadratic approximation of the phase terms in the PO integrand was discussed in [17]–[21], [31], [32], and [36]. In [17] and [18], when the PO integrand has a quadratic phase, an exact closed form formula is derived. And when the general type PO integrand is considered, the asymptotic evaluation is proposed without any approximation for the amplitude and phase functions. Closed-form formula in terms of the special generalized Fresnel and UTD transition functions is proposed. In [3], [32], [36], [37], the steepest descent path deformation technique in the complex plane is adopted to handle this type of highly oscillatory PO integrals on the NSDPs.

The paper is organized as follows. First, we derive the PO scattered field on smooth conducting surfaces. The amplitude and phase functions of the PO integrand are approximated by quadratic functions. Then, the affine transformations are used to simplify the PO integral to its canonical forms on each triangular patch. Next, this PO double integral is reduced into several highly oscillatory line integrals, and the NSDP method is employed to rewrite these PO integrals on the corresponding NSDPs. After that, through combining the PO integral on each triangular patch, the PO scattered field is expressed on the assembled triangular patches. Finally, numerical examples on the parabolic patch are given to verify the proposed NSDP method.

II. PO Surface Integral Formulation

When a perfect conducting object is excited by an external source, the electromagnetic (EM) scattered fields can be expressed by the Stratton-Chu integral formulas [4]. For the observation point far away from the considered object, the far scattered electric field is expressed as

$$\mathbf{E}_s(\mathbf{r}) \approx -\frac{ikZ_0e^{ikr}}{4\pi r}\hat{\mathbf{r}}\times\hat{\mathbf{r}}\times\int_{\partial\Omega} dS(\mathbf{r}')\left[\hat{\mathbf{n}}(\mathbf{r}')\times\mathbf{H}(\mathbf{r}')\right]e^{-ik\hat{\mathbf{r}}\cdot\mathbf{r}'} \tag{1}$$

where $\partial\Omega$ is the boundary of the object, k is the wave number outside Ω, ω is the angular frequency, $\mathbf{r}$ is the observation point with the amplitude r and unit vector $\hat{\mathbf{r}}$, $\mathbf{r}'$ is the surface point on $\partial\Omega$, $\hat{\mathbf{n}}(\mathbf{r}')$ is the outward unit normal vector of $\partial\Omega$, Z_0 is the free space intrinsic impedance constant. EM fields are time harmonic with the time dependence $e^{-i\omega t}$.

When the working frequency k of the wave field is high enough, the surface induced PO current [6], [8] on the surface of the object is approximated by

$$\mathbf{J}(\mathbf{r}') = \begin{cases} 2\hat{\mathbf{n}}(\mathbf{r}')\times\mathbf{H}^{(i)}(\mathbf{r}'), & \mathbf{r}'\in\partial\Omega_1 \\ 0, & \mathbf{r}'\in\partial\Omega_2 \end{cases} \tag{2}$$

where $\partial\Omega_1$ and $\partial\Omega_2$ are the lit and shadow regions of $\partial\Omega$, respectively. For notation simplification, in the following, we still use $\partial\Omega$ to represent the lit region of the considered object. $\mathbf{H}^{(i)}(\mathbf{r}')$ is the incident magnetic field on $\partial\Omega$. In particular, we choose the plane incident wave

$$\mathbf{E}^{(i)}(\mathbf{r}) = \mathbf{E}_0^{(i)}e^{ik\hat{\mathbf{r}}^{(i)}\cdot\mathbf{r}}, \quad \mathbf{H}^{(i)}(\mathbf{r}) = \frac{\hat{\mathbf{r}}^{(i)}\times\mathbf{E}_0^{(i)}}{Z_0}e^{ik\hat{\mathbf{r}}^{(i)}\cdot\mathbf{r}}. \tag{3}$$

Then, after substituting (2) and (3) into (1), the far scattered electric field can be represented by a surface integral [36]

$$\mathbf{E}_s(\mathbf{r}) \approx \int_{\partial\Omega} dS(\mathbf{r}')\mathbf{s}_{\rm bi}(\mathbf{r}')e^{ikv_{\rm bi}(\mathbf{r}')} \tag{4}$$

with

$$\mathbf{s}_{\rm bi}(\mathbf{r}') = -\frac{ike^{ikr}}{2\pi r}\hat{\mathbf{r}}\times\hat{\mathbf{r}}\times\left(\hat{\mathbf{n}}(\mathbf{r}')\times\hat{\mathbf{r}}^{(i)}\times\mathbf{E}_\mathbf{0}^{(i)}\right) \tag{5}$$

$$v_{\rm bi}(\mathbf{r}') = \left(\hat{\mathbf{r}}^{(i)}-\hat{\mathbf{r}}\right)\cdot\mathbf{r}'. \tag{6}$$

The equation above is the bistatic scattered electric field under the PO approximation, which is called the PO integral. $\mathbf{E}_0^{(i)}$ in (3) is the incident electric polarization wave vector. In (5) and (6), $\mathbf{s}_{\rm bi}(\mathbf{r}')$ is the vector amplitude function which is usually slowly varying when the surface of the object is smooth. The exponential of the phase function term, $e^{ikv_{\rm bi}(\mathbf{r}')}$, will become highly oscillatory as the working frequency k increases.

In particular, for the monostatic case with $\hat{\mathbf{r}} = -\hat{\mathbf{r}}^{(i)}$, the PO surface integral in (4) can be represented as [36]

$$\mathbf{E}_s(\mathbf{r}) \approx \mathbf{E}_0^{(i)}\tilde{I}_{\rm mono} \tag{7}$$

with

$$\tilde{I}_{\rm mono} = \int_{\partial\Omega} dS(\mathbf{r}')s_{\rm mono}(\mathbf{r}')e^{ikv_{\rm mono}(\mathbf{r}')} \tag{8}$$

$$s_{\rm mono}(\mathbf{r}') = -\frac{ike^{ikr}}{2\pi r}\hat{\mathbf{r}}^{(i)}\cdot\hat{\mathbf{n}}(\mathbf{r}'), v_{\rm mono}(\mathbf{r}') = 2\hat{\mathbf{r}}^{(i)}\cdot\mathbf{r}'. \tag{9}$$

Compared (9) with (5), the amplitude function now is simplified into a scalar function $s_{\rm mono}(\mathbf{r}')$. Furthermore, from (4), (7), $\mathbf{E}_s(\mathbf{r})$ under the PO approximation for both the bistatic and monostatic cases takes the general form

$$\tilde{I} = \int_{\partial\Omega} dS(\mathbf{r}')s(\mathbf{r}')e^{ikv(\mathbf{r}')}. \tag{10}$$

Here, the amplitude and phase terms are denoted as $s(\mathbf{r}')$ and $v(\mathbf{r}')$, respectively.

III. Motivation of the PO Formulation

In (10), we see that the PO kernel contains the amplitude and phase function terms. If the amplitude and phase functions are linearly varying, then the PO integral defined on the flat polygon patches can be solved in closed form [28], [29]. However, the PO kernel with linear phase term cannot yield the contributions of stationary phase points, and resonance points in physics.

In this work, we propose the PO integrand with quadratic phase to capture the contributions of critical points. The corresponding geometry surface $\partial\Omega$ in (10) is the quadratic patch. Then, the PO integrand exactly takes the form of quadratic variations of the amplitude and phase functions. Since an arbitrary curved surface can be discretized into a number of quadratic triangles, the geometry errors shall be much smaller than those generated by the same number of flat triangular patches. Hence, this natural extension shall be an important application for the proposed method used on the real-world objects. For the highly oscillatory PO integral with quadratic variations of both the amplitude and phase terms, we propose an efficient numerical steepest descent path method to evaluate it. Specifically, the workload for the PO surface integral defined on the quadratic patch is independent of wave frequency. In the following, we discuss the proposed algorithm procedure in detail.

IV. The Quadratic Polynomial Approximation of the Amplitude and Phase Functions

We assume that the surface of the object $\partial\Omega$ is governed by equation $z = f(x, y)$, and its projection onto the $x - y$ plane is $\partial\Omega_{xy}$. Then we use M triangular patches to discretize the domain $\partial\Omega_{xy}$, that is, $\triangle_1, \triangle_2, \cdots, \triangle_M$. To capture the stationary phase and resonance points of the PO integrand in (10), we approximate the amplitude and phase functions by the second order polynomials on these triangular patches. Hence, the PO integral $\tilde{I}$ in (10) can be expressed as

$$\begin{aligned}\tilde{I} &= \int_{\partial\Omega_{xy}} \tilde{s}(x,y)e^{ik\tilde{v}(x,y)}t(x,y)dxdy \\ &= \sum_{n=1}^{M}\int_{\triangle_n} \tilde{d}(x,y)e^{ik\tilde{v}(x,y)}dxdy \\ &\simeq \sum_{n=1}^{M}\int_{\triangle_n} \tilde{d}_n(x,y)e^{ik\tilde{v}_n(x,y)}dxdy \end{aligned} \tag{11}$$

where

$$\begin{aligned}&\tilde{s}(x,y) = s\left(x,y,f(x,y)\right),\ \tilde{v}(x,y) = v\left(x,y,f(x,y)\right) \\ &t(x,y) = \sqrt{1+\left[f_x(x,y)\right]^2+\left[f_y(x,y)\right]^2} \\ &\tilde{d}(x,y) = \tilde{s}(x,y)t(x,y).\end{aligned}$$

Here, the number of triangles M in (11) depends on the electrical size of the considered object, the wave frequency of interest, and also the curvature radii of the surface of the object. The second order polynomials $\tilde{d}_n(x,y)$ and $\tilde{v}_n(x,y)$ in (11) are the approximated amplitude and phase functions. They can be obtained by the Lagrange interpolation polynomial approximation [33] of $\tilde{d}(x,y)$ and $\tilde{v}(x,y)$ on these triangular patches $\triangle_n$, $n = 1, 2, \cdots, M$. Their formulas are

$$\begin{aligned}\tilde{v}_n(x,y) =& \tilde{\beta}_{n,1}+\tilde{\beta}_{n,2}x+\tilde{\beta}_{n,3}y+\tilde{\beta}_{n,4}x^2+\tilde{\beta}_{n,5}y^2 \\ &+\tilde{\beta}_{n,6}xy, \end{aligned} \tag{12}$$

$$\begin{aligned}\tilde{d}_n(x,y) =& \tilde{\alpha}_{n,1}+\tilde{\alpha}_{n,2}x+\tilde{\alpha}_{n,3}y+\tilde{\alpha}_{n,4}x^2+\tilde{\alpha}_{n,5}y^2 \\ &+\tilde{\alpha}_{n,6}xy \end{aligned} \tag{13}$$

with coefficients $\tilde{\beta}_{n,m} \in \mathbb{C}$, $\tilde{\alpha}_{n,m} \in \mathbb{R}$, $m = 1, 2, \cdots, 6$. However, for the quadratic patch, the surface $z = f(x, y)$ is governed by a second order polynomial. Then, the corresponding $\tilde{v}(x,y)$ and $\tilde{d}(x,y)$ in (11) are exact and can be rigorously derived as the quadratic polynomials.

Furthermore, after some affine transformations, the quadratic phase function $\tilde{v}_n(x,y)$ in each summation integral term in (11) has the simplified canonical form. In this manner, each summation integral term in (11) can be reformulated to

$$I_n = \int_{\triangle'_n} \tilde{p}_n(x',y')e^{ik\left[\pm(x')^2\pm(y')^2\right]}dx'dy' \tag{14}$$

where

$$\tilde{p}_n(x',y') = \tilde{d}_n\left(x(x',y'),y(x',y')\right)e^{ik\tilde{G}_n}|\mathbf{Q}_n| \tag{15}$$

is also a second order polynomial in the $x' - y'$ coordinate system, and

$$\mathbf{Q}_n = \left[\frac{\partial(x,y)}{\partial(x',y')}\right]_{(\triangle_n\to\triangle'_n)}$$

is the Jacobi coordinate transform matrix between two coordinate systems $x-y$ and $x'-y'$. Detailed derivations are presented in Appendix A. The above canonical expression (14) is valid for both monostatic and bistatic cases.

Due to the highly oscillatory behavior of the canonical form PO integral I_n in (14), if one evaluates it accurately by the direct numerical scheme, such as the adaptive Simpson's rule, the number of discretized triangle meshes in (11) shall increase as $M = M(k) \sim O(k^2)$. In the following, we will propose a NSDP method to k-independently evaluate the canonical PO integral I_n in (14).

V. Analyzing the Surface PO Integral by the Numerical Steepest Descent Path Method

We start with the surface PO integral in (10). After the affine transformation in Section III, the canonical PO surface integral I_n on each triangular patch is expressed in (14). It can be reduced into three highly oscillatory line integrals [36] on the three edges of each triangular patch. Then, we develop a NSDP method for calculating the reduced highly oscillatory line integral defined on an arbitrary edge of a triangular patch. Finally, the expressions of the PO scattered electric field on the assembled triangles are presented based on the NSDPs. In the following, we describe the main procedure.

A. Reduction of the Double PO Integral into the Highly Oscillatory Line Integrals

We consider the canonical highly oscillatory PO integrand in (14) defined on the domain $[L_1, L_2] \times [0, ax + b]$ (Fig. 1). That is

$$\begin{aligned}I^{(a,b)} &= \int_{L_1}^{L_2}\int_0^{ax+b} p(x,y)e^{ik(x^2+y^2)}dydx \\ &= \int_{L_1}^{L_2} e^{ikx^2}F(x)dx. \end{aligned} \tag{16}$$

Here, we assume $ax + b > 0$, and $p(x,y)$ has the similar form as $\tilde{d}_n(x,y)$ in (13), with coefficients α_m, $m = 1, 2, \cdots, 6$. In (16), $F(x)$ has the formula

$$\begin{aligned}F(x) &= \int_0^{ax+b} p(x,y)e^{iky^2}dy \\ &= j_2^{(a,b)}(x)e^{ik(ax+b)^2} \\ &\quad - j_2^{(0,0)}(x)+j_1(x)\left[\text{erfc}\left(\sqrt{-ik}(ax+b)\right)-1\right] \end{aligned} \tag{17}$$

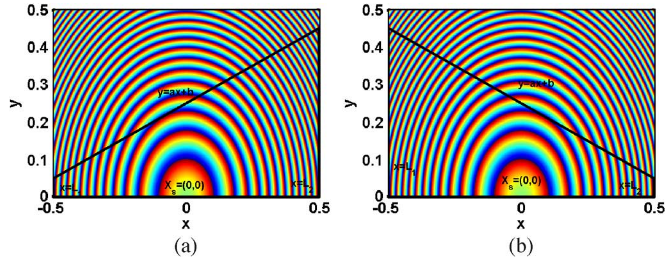

Fig. 1. Integration domains $[L_1, L_2] \times [0, ax+b]$ for the highly oscillatory integrand of (16) with $a > 0$ (a) and $a < 0$ (b).

where

$$j_1(x) = -\frac{\sqrt{\pi}}{2\sqrt{-ik}}\left(\alpha_1 + \alpha_2 x + \alpha_4 x^2 - \frac{\alpha_5}{2ik}\right)$$
$$j_2^{(a,b)}(x) = \frac{\alpha_3 + \alpha_6 x + \alpha_5(ax+b)}{2ik}$$
$$j_2^{(0,0)}(x) = \frac{\alpha_3 + \alpha_6 x}{2ik}.$$

The complementary error function $\mathrm{erfc}(z)$ [34] is defined by

$$\mathrm{erfc}(z) = \frac{2}{\sqrt{\pi}}\int_z^\infty e^{-t^2}dt.$$

Furthermore, $F(x)$ in (17) can be decomposed into two different parts defined on the edges $y = 0$ and $y = ax + b$

$$F(x) = J_2^{(a,b)}(x) - J_2^{(0,0)}(x) \tag{18}$$

where

$$J_2^{(0,0)}(x) = j_1(x) + j_2^{(0,0)}(x)$$
$$J_2^{(a,b)}(x) = j_1(x)\mathrm{erfc}\left(\sqrt{-ik}(ax+b)\right) + j_2^{(a,b)}(x)e^{ik(ax+b)^2}.$$

By substituting (18) into (16), the integral $I^{(a,b)}$ is split into two parts

$$I^{(a,b)} = I_2^{(a,b)} - I_2^{(0,0)} \tag{19}$$

where

$$I_2^{(0,0)} = \int_{L_1}^{L_2} J_2^{(0,0)}(x)e^{jkx^2}dx \tag{20}$$

has the closed-form formula in terms of the complementary error function [36]. But meanwhile

$$I_2^{(a,b)} = \int_{L_1}^{L_2} J_2^{(a,b)}(x)e^{jkx^2}dx \tag{21}$$

is a highly oscillatory integral that cannot be solved analytically. Due to the asymptotic behavior and Stokes' phenomenon of $\mathrm{erfc}(z)$ [34], [36], the phase variation of the integrand in $I_2^{(a,b)}$ is

$$g(x) = x^2 + (ax+b)^2. \tag{22}$$

In the next subsection, we will introduce the NSDP method to handle the highly oscillatory integral $I_2^{(a,b)}$.

B. Numerical Steepest Descent Path Method for $I_2^{(a,b)}$

Given the integration domain $[L_1, L_2]$ shown in Fig. 1, we define the path functions $x = x_{L_m}(p)$, $m = 1, 2$, $p \in [0, \infty)$, satisfying three conditions [3]:

(a) $x_{L_m}(0) = L_m$, that is, the paths start at L_m;
(b) $\mathrm{Re}(g(x_{L_m}(p))) = \mathrm{Re}(g(x_{L_m}(0))) \equiv C$, where C is a constant;
(c) $\mathrm{Im}(g(x_{L_m}(p))) = p$.

The phase term $g(x)$ of $I_2^{(a,b)}$ in the above conditions (a)–(c) is given in (22). Then, after substituting $x = x_{L_m}(p)$ into the phase function, we see that $e^{ikg(x_{L_m}(p))} = e^{ikg(L_m)-kp}$ decrease exponentially as $O(e^{-kp})$ when p goes large. Hence, we call the path functions $x = x_{L_m}(p)$ by the NSDPs. Through (a), (b), and (c), we have [3], [36]

$$x_{L_m}(p)^2 + (ax_{L_m}(p) + b)^2 = L_m^2 + (aL_m + b)^2 + ip. \tag{23}$$

After reformulating the above (23), the NSDPs for the end points L_m are

$$x_{L_m}(p) = \frac{\mathrm{sgn}\,(L'_m)}{\sqrt{1+a^2}}\sqrt{{L'_m}^2 + ip} + x_s, p \in [0, \infty) \tag{24}$$

where $L'_m = \sqrt{1+a^2}(L_m - x_s)$, and the stationary phase point $x_s = -(ab/(1+a^2))$ satisfies $g'(x_s) = 0$.

However, the NSDP for the stationary phase point shall change in the following way. We notice that the Taylor expansion of the phase function at the stationary phase point x_s is

$$g(x) - g(x_s) \approx \frac{(x-x_s)^2}{2!}g''(x_s) + O\left((x-x_s)^3\right), \quad x \to x_s.$$

It means that $g(x) - g(x_s)$ is a quadratic function around x_s [3]. Hence, we change the above condition (c) with $\mathrm{Im}(g(x_{L_m}(p))) = p^2$, and define the corresponding NSDP, $x = x_0(p)$, $p \in (-\infty, \infty)$, such that

$$x_0(p)^2 + (ax_0(p) + b)^2 = x_s^2 + (ax_s + b)^2 + ip^2. \tag{25}$$

The explicit NSDP formula $x_0(p)$ can be got from the above (25) as

$$x_0(p) = \frac{e^{\left(i\frac{\pi}{4}\right)}p}{\sqrt{1+a^2}} + x_s, p \in (-\infty, \infty). \tag{26}$$

Fig. 3 shows that the NSDPs defined on the four edges of the quadrilateral domain shown in Fig. 2. For example, Fig. 3(a) gives the NSDPs for the integrand $I_2^{(a_1,b_1)}$ defined on the edge $\overrightarrow{\mathbf{V}_1\mathbf{V}_2}$ as shown in Fig. 2. The edge $\overrightarrow{\mathbf{V}_1\mathbf{V}_2}$ is governed by the equation $y = a_1x + b_1$. $x_{L_1}^{(1)}(p)$, $x_{L_2}^{(1)}(p)$ and $x_0^{(1)}(p)$ are the NSDPs for the two end points, and the stationary phase point, respectively. The corresponding integration end points and stationary phase point are $L_1 = \mathbf{V}_1(1)$, $L_2 = \mathbf{V}_2(1)$, and $x_s = -(a_1b_1/1 + a_1^2)$. Here, $\mathbf{V}_m = (\mathbf{V}_m(1), \mathbf{V}_m(2))$, $m = 1, 2, 3, 4$. Due to the intrinsic Stokes' phenomenon of $\mathrm{erfc}(z)$ [34], the resultant Stokes' line is expressed by equation $y = -x - (b_1/a_1)$ [36]. The intersection points of the Stokes' line with the NSDPs $x_0^{(1)}(p)$ and $x_{L_1}^{(1)}(p)$ are $\mathbf{A}^{(1)}$ and $\mathbf{B}^{(1)}$. We notice that the integrand of $I_2^{(a_1,b_1)}$ expressed in (21), i.e.,

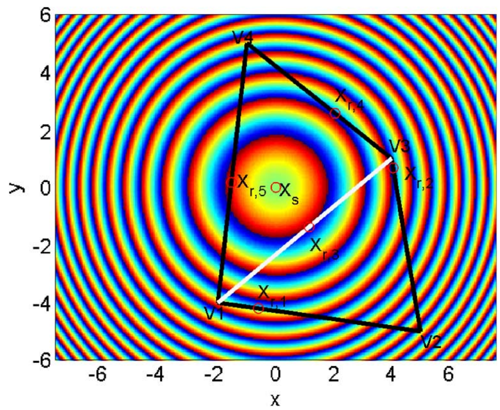

Fig. 2. The $x-y$ quadrilateral domain $\mathbf{V}_1\mathbf{V}_2\mathbf{V}_3\mathbf{V}_4$.

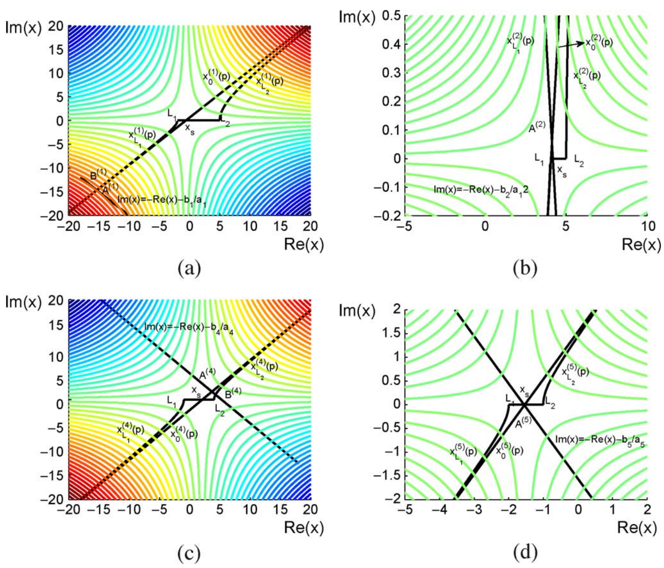

Fig. 3. Subfigures (a), (b), (c), (d) correspond to the numerical steepest descent paths for the integrand of $I_2^{(a_m,b_m)}$, $m=1,2,4,5$, defined on the four edges in Fig. 2. The edges are governed by $y=a_mx+b_m$, the phase functions on the edges are $g^{(m)}(x)=x^2+(a_mx+b_m)^2$, and the Stokes' lines are $y=-x-(b_m/a_m)$. The integration end points L_1 and L_2 are the x-values of the end points on the corresponding four edges. The intersection points of the Stokes' lines and the NSDPs are $\mathbf{A}^{(m)}$ and $\mathbf{B}^{(m)}$. The x-axis points x_s correspond to the stationary phase points of the phase terms $g^{(m)}(x)$. The resonance points on edges m are $\mathbf{X}_{r,m}=(x_s,a_mx_s+b_m)$, $m=1,2,4,5$.

$J_2^{(a_1,b_1)}(x)e^{ikx^2}$, is analytic. Thus, by applying Cauchy's integral theorem, we rewrite $I_2^{(a_1,b_1)}$ on the NSDPs [36]

$$I_2^{(a_1,b_1)} = \int_{x_{\mathrm{NSDP}}(p)} J_2^{(a_1,b_1)}(x)e^{ikx^2}dx = \underbrace{\int_{x_{\mathrm{NSDP}}(p)} f^{(1)}(x)e^{ikg^{(1)}(x)dx}}_{I_{2,\mathrm{NSDP}}^{(a_1,b_1)}} + \underbrace{\int_{x_{l_*}} 2j_1(x)e^{ikx^2}dx}_{I_{2,\mathrm{analytic}}^{(a_1,b_1)}}, \tag{27}$$

where

$$f^{(1)}(x) = j_1(x)E^c(x) + j_2^{(a_1,b_1)}(x) \tag{28}$$

is a slowly varying function, and $E^c(x)$ relates to the slowly varying part of the complementary error function [36]. Here, $g^{(1)}(x)$ is the phase term by substituting (a_1,b_1) into (22). The approximation in (27) is made since the asymptotic approximation of the complementary error function holds when its argument goes to infinity. Again by using Cauchy's integral theorem, $I_{2,\mathrm{NSDP}}^{(a_1,b_1)}$ has the expression

$$I_{2,\mathrm{NSDP}}^{(a_1,b_1)} = I_{L_1}^{(a_1,b_1)} - I_{L_2}^{(a_1,b_1)} + I_{x_s}^{(a_1,b_1)} \tag{29}$$

$$I_{L_m}^{(a_1,b_1)} = \int_0^\infty e^{-kp}e^{ikg^{(1)}(L_m)}f^{(1)} \times \left(x_{L_m}^{(1)}(p)\right)\left(x_{L_m}^{(1)}(p)\right)'dp \tag{30}$$

$$I_{x_s}^{(a_1,b_1)} = \int_{-\infty}^{\infty} e^{-kp^2}e^{ikg^{(1)}(x_s)}f^{(1)} \times \left(x_0^{(1)}(p)\right)\left(x_0^{(1)}(p)\right)'dp \tag{31}$$

and $m=1,2$. Furthermore, the integrand of $I_{2,\mathrm{analytic}}^{(a_1,b_1)}$ in (27), i.e., $2j_1(x)e^{ikx^2}$, has an antiderivative $K(x)$ with the formula

$$K(x) = \left(-\frac{\pi}{2ik}\alpha_1 - \frac{\pi}{4k^2}\alpha_4 - \frac{\pi}{4k^2}\alpha_5\right)\mathrm{erfc}\left(\sqrt{-ik}x\right) + \left(-\frac{\sqrt{\pi}}{2ik\sqrt{-ik}}\alpha_2 - \frac{\sqrt{\pi}x}{2ik\sqrt{-ik}}\alpha_4\right)e^{ikx^2}. \tag{32}$$

The integrand $2j_1(x)e^{ikx^2}$ in $I_{2,\mathrm{analytic}}^{(a_1,b_1)}$ comes from the Stokes' phenomenon of $\mathrm{erfc}(z)$ [36]. The integral path x_{l_*} in (27) is related to the intersection points between the Stokes' line $y=-x-(b_1/a_1)$ and $x_{\mathrm{SDP}}(p)$. By applying Cauchy's integral theorem and based on Fig. 3(a), we have

$$\begin{aligned} I_{2,\mathrm{analytic}}^{(a_1,b_1)} &= \int_{(\mathbf{V}_1(1),0)}^{(\mathbf{V}_2(1),0)} 2j_1(x)e^{ikx^2}dx - \int_{\mathbf{A}^{(1)}}^{\mathbf{B}^{(1)}} 2j_1(x)e^{ikx^2}dx \\ &= K((\mathbf{V}_2(1),0)) - K((\mathbf{V}_1(1),0)) - K\left(\mathbf{B}^{(1)}\right) + K\left(\mathbf{A}^{(1)}\right). \end{aligned} \tag{33}$$

C. Representation of the PO Integral on the Assembled Triangular Patches by the Numerical Steepest Descent Path Method

We give the expression of $I_2^{(a_1,b_1)}$ in (27), which is defined on the edge $\overrightarrow{\mathbf{V}_1\mathbf{V}_2}$ in Fig. 3(a). By invoking "(54–57)" in [36], the PO scattered surface integral $\tilde{I}$ expressed in (11) can be represented in terms of the NSDPs

$$\tilde{I} = -I_2^{(a_1,b_1)} + I_2^{(a_2,b_2)} + I_2^{(a_4,b_4)} + I_2^{(a_5,b_5)} \tag{34}$$

where

$$I_2^{(a_2,b_2)} = I_{L_1}^{(a_2,b_2)} + I_{x_s}^{(a_2,b_2)} - I_{L_2}^{(a_2,b_2)} + K((\mathbf{V}_2(1),0)) - K\left(\mathbf{A}^{(2)}\right) \tag{35}$$

$$I_2^{(a_4,b_4)} = I_{L_1}^{(a_4,b_4)} + I_{x_s}^{(a_4,b_4)} - I_{L_2}^{(a_4,b_4)} + K\left(\mathbf{B}^{(4)}\right) - K\left(\mathbf{A}^{(4)}\right) \tag{36}$$

$$I_2^{(a_5,b_5)} = I_{L_1}^{(a_5,b_5)} + I_{x_s}^{(a_5,b_5)} - I_{L_2}^{(a_5,b_5)} + K\left(\mathbf{A}^{(5)}\right) - K((\mathbf{V}_1(1),0)). \tag{37}$$

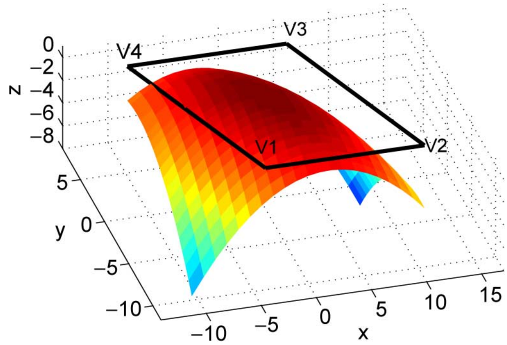

Fig. 4. Parabolic PEC patch.

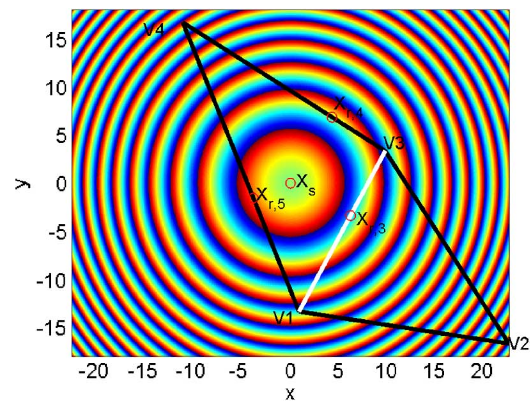

Fig. 5. The $x-y$ quadrilateral domain $\mathbf{V}_1\mathbf{V}_2\mathbf{V}_3\mathbf{V}_4$ of the parabolic PEC patch shown in Fig. 4.

Originally, $I_2^{(a_m,b_m)}$, $m=2,4,5$, are the highly oscillatory PO line integrals $I_2^{(a,b)}$ defined on the three edges $\overrightarrow{\mathbf{V}_2\mathbf{V}_3}$, $\overrightarrow{\mathbf{V}_3\mathbf{V}_4}$ and $\overrightarrow{\mathbf{V}_1\mathbf{V}_4}$ in Fig. 2. Now they are expressed in terms of NSDPs. Here, $I_{2,\mathrm{analytic}}^{(a_m,b_m)}$, $m=2,4,5$, have closed-form formulas and follow the similar derivation procedure as (33). **Remark 1**. In the **Proposition 1** of [36], we have given the proof that the internal resonance point contribution to the PO integral $\tilde{I}$ by the NSDP method is 0. Here, the edge $\overrightarrow{\mathbf{V}_1\mathbf{V}_3}$ in Fig. 2 contains an internal resonance point, and its contribution to the PO integral $\tilde{I}$ is 0. Also, when $\tilde{I}$ in (11) is calculated in the two triangular patches $\triangle_{\mathbf{V}_1\mathbf{V}_2\mathbf{V}_3}$ and $\triangle_{\mathbf{V}_1\mathbf{V}_3\mathbf{V}_4}$, the contribution of $I_2^{(a_3,b_3)}$ is calculated twice with different signs. Thus, in (34), the contribution $I_2^{(a_3,b_3)}$ to PO integral $\tilde{I}$ is 0. That is the reason why we use the white line in Fig. 2 to denote $\overrightarrow{\mathbf{V}_1\mathbf{V}_3}$.

VI. Numerical Results

We consider the PEC parabolic patch

$$f(x,y,z): z = 1 - 0.06(x^2+xy+y^2), \tag{38}$$

presented in [17] to benchmark our proposed NSDP method. It is shown in Fig. 4.

A. The Assembled Triangular Patches Example

The surface is trimmed on the quadrilateral domain in the $x-y$ plane as shown in Fig. 5, with the four corners $\mathbf{V}_1 = (0.8932, -13.3333)$, $\mathbf{V}_2 = (22.7671, -16.6667)$, $\mathbf{V}_3 = (9.8803, 3.3333)$, and $\mathbf{V}_4 = (-11.2201, 16.6667)$. We set the parameters as follows: the frequency $k \in [100, 1000]$, the incident wave propagates along $-z$ direction, i.e., $\hat{\mathbf{r}}^{(i)} = (0,0,-1)$. We consider the far-field and backward scattering case. In Fig. 5, the quadrilateral domain $\mathbf{V}_1\mathbf{V}_2\mathbf{V}_3\mathbf{V}_4$ is decomposed into two triangular domains $\triangle_{\mathbf{V}_1\mathbf{V}_2\mathbf{V}_3}$ and $\triangle_{\mathbf{V}_1\mathbf{V}_3\mathbf{V}_4}$. When $z_0 > 0$, the matrix

$$\mathbf{W}_n = \begin{bmatrix} \tilde{\beta}_{n,4} & \frac{\tilde{\beta}_{n,6}}{2} \\ \frac{\tilde{\beta}_{n,6}}{2} & \tilde{\beta}_{n,5} \end{bmatrix} = 0.06 z_0 \begin{bmatrix} 1 & \frac{1}{2} \\ \frac{1}{2} & 1 \end{bmatrix}, \quad n = 1,2$$

defined in (41) (see Appendix A) is symmetric and positive-definite. Hence, $e^{ik\tilde{v}_n(x,y)}$ can be simplified to $e^{ik(x^2+y^2)}$ as that in Section III. After the affine transformation in (46), the quadrilateral domain in Fig. 5 is transformed to the quadrilateral domain in Fig. 2. We apply the Gauss–Legendre quadrature to calculate these integrals defined on the NSDPs by using (33)–(37).

TABLE I

Comparisons of the RCS Values (dBsm Unit) Produced and the CPU Time (Second Unit) Consumed by Using the NSDP Method and the Brute Force (BF) Method to Calculate the Scattered Electric Field as Given in (7)

Frequency k	BF–RCS	NSDP–RCS	BF–CPU	NSDP–CPU
100	24.577195	24.573213	4.8984	3.9780
300	24.705320	24.704920	14.4769	3.9000
500	24.684031	24.685079	24.3050	4.0092
800	24.675256	24.679175	38.8598	3.9780
1000	24.664418	24.667404	48.7815	4.0404

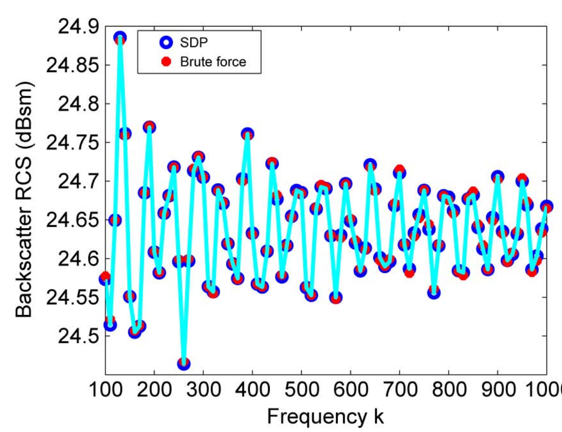

Fig. 6. Comparisons of the RCS (dBsm unit) values of the PO scattered electric field (7) by the NSDP method and the brute force method.

In Table I, through the brute force method verification results, we show the error-controllable PO scattered electric field results produced by the NSDP method in the second and third columns. Then, we give the comparisons of the CPU time (second unit) consumed by both methods in the fourth and fifth columns. We conclude that the proposed NSDP method is frequency-independent and error-controllable. To see the conclusion more clearly, Fig. 6 demonstrates the RCS values (dBsm unit) of the PO scattered electric field $\mathbf{E}_s(\mathbf{r})$ by both methods. We see that the results produced by both methods agree well with each other. Furthermore, Fig. 7 shows that the CPU time consumed by the

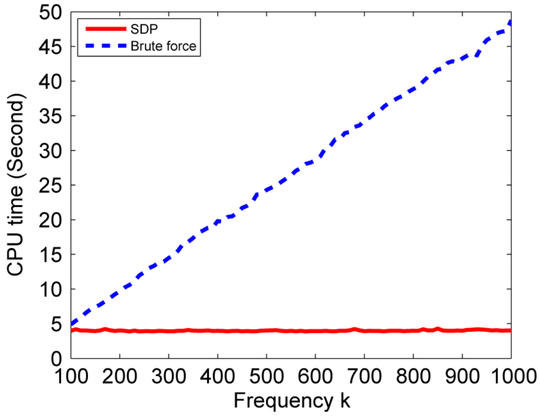

Fig. 7. Comparisons of the CPU time (second unit) for the PO scattered electric field (7) by using the NSDP method and the brute force method.

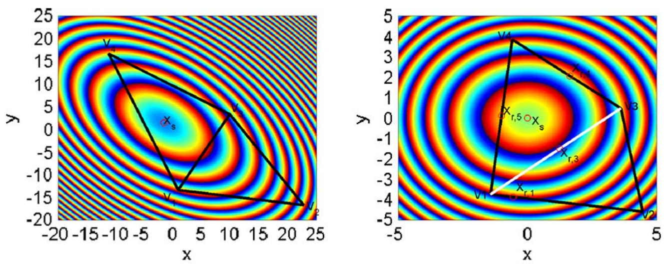

(a) (b)

Fig. 8. (a): The $x-y$ quadrilateral domain $\mathbf{V}_1\mathbf{V}_2\mathbf{V}_3\mathbf{V}_4$ of the parabolic PEC patch shown in Fig. 4. (b): The $x-y$ affine transformed quadrilateral domain from (a).

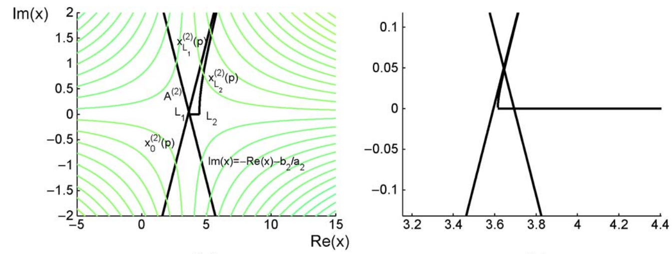

(a) (b)

Fig. 9. (a): Steepest descent paths for the integrand of $I_2^{(a_2,b_2)}$ defined on edge $2-\mathbf{V}_2\mathbf{V}_3$ with the equation $y=a_2x+b_2$. The phase function on the edge is $g_2(x)=x^2+(a_2x+b_2)^2$. The Stokes' line is $y=-x-(b_2/a_2$. The integration end points are $L_1=\mathbf{V}_3(1)$, $L_2=\mathbf{V}_2(1)$. The intersection points of the Stokes' line and the NSDP $x_0^{(2)}(p)$ is $\mathbf{A}^{(2)}$. x_s corresponds to the stationary phase point of $g_2(x)$. (b): Zoomed in subfigure from Fig. 9(a).

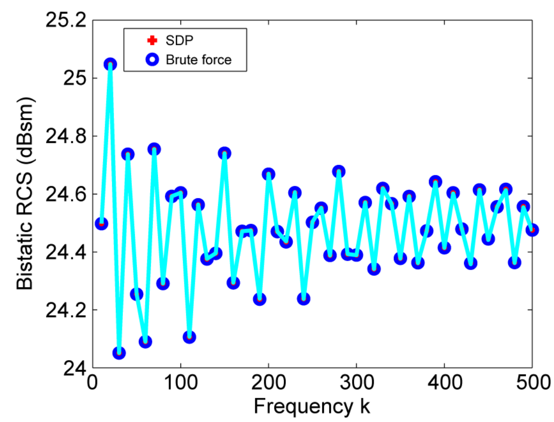

Fig. 10. Comparisons of the RCS (dBsm unit) values of the PO scattered electric field (1) by the NSDP method and the brute force method.

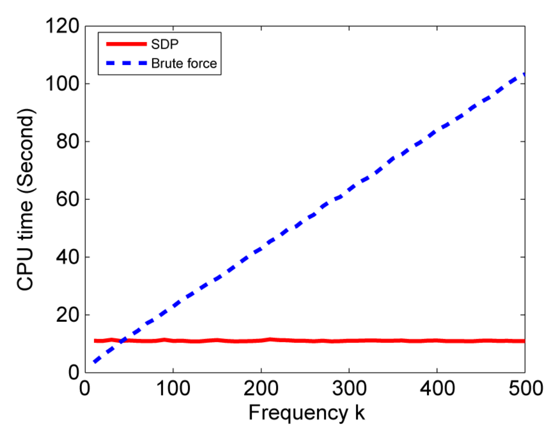

Fig. 11. Comparisons of the CPU time (second unit) for the PO scattered electric field (1) by using the NSDP method and the brute force method.

NSDP method for calculating the PO scattered electric field is frequency-independent as that in [35].

The NSDP method can also be applied for calculating the PO integral in (4) with the bistatic case. We set the parameters: the frequency $k\in[10,500]$, the incident wave propagates along $\hat{\mathbf{r}}^{(i)}=[0.5,0.5,-\sqrt{2}/2]$ direction, the observation point is set along the unit direction $\hat{\mathbf{r}}=[\sqrt{2}/4,\sqrt{6}/4,\sqrt{2}/2]$, the incident electric wave has polarization amplitude $\mathbf{E}_0^{(i)}=[-\sqrt{2}/2,\sqrt{2}/2,0]$ with $\mathbf{E_0}^{(i)}\cdot\hat{\mathbf{r}}^{(i)}=0$. In this case, the parabolic patch in Fig. 4 is trimmed on the quadrilateral domain in the $x-y$ plane as shown in Fig. 8(a). Compared with the above monostatic example, the different parts for calculating the bistatic scattered electric field in (4) by the NSDP method are:

1) The bistatic scattered electric field expressed by (4) is a vector function with three highly oscillatory PO type integrals now, and shall be calculated three times by using the NSDP method. This is different from the scalar highly oscillatory PO type integral in (8).
2) Due to the bistatic parameters of the source and observation points, the stationary phase point $\mathbf{X}_s=[0,0]^T$ in Fig. 5 changes to $\mathbf{X}_s=[-1.5920,1.4582]^T$ in Fig. 8(a). Hence, the phase function $v(\mathbf{r}')$ in (10) is different from that in monostatic case.
3) Since the phase function in the PO integrand changed, the corresponding numerical steepest descent paths defined on the four edges in Fig. 8(b) shall also change. For example, the NSDPs for edge $2-\overrightarrow{\mathbf{V}_2\mathbf{V}_3}$ in Fig. 3(b) change to that in Fig. 9(a). Hence, the corresponding $I_2^{(a_2,b_2)}$ in (35) changes to the following equation:

$$I_2^{(a_2,b_2)}=I_{L_1}^{(a_2,b_2)}-I_{L_2}^{(a_2,b_2)}+K\left((\mathbf{V}_2(1),0)\right)-K\left(\mathbf{A}^{(2)}\right). \tag{39}$$

By using the NSDP method, Figs. 10, 11 again demonstrate the error-controllable and frequency-independent bistatic PO scattered field results.

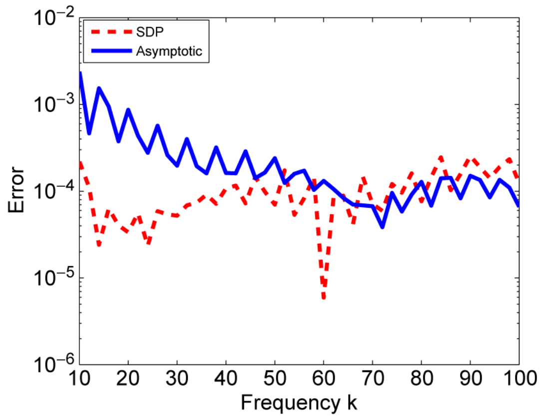

Fig. 12. Red line: The relative error of the monostatic scattered electric field $\mathbf{E}_s(\mathbf{r})$ results [see (7)] produced by using the NSDP method relative to the brute force method on the parabolic patch. Blue line: The relative error of the monostatic scattered electric field $\mathbf{E}_s(\mathbf{r})$ results [see (7)] produced by using the asymptotic expansion method [17] relative to the brute force method on the parabolic patch.

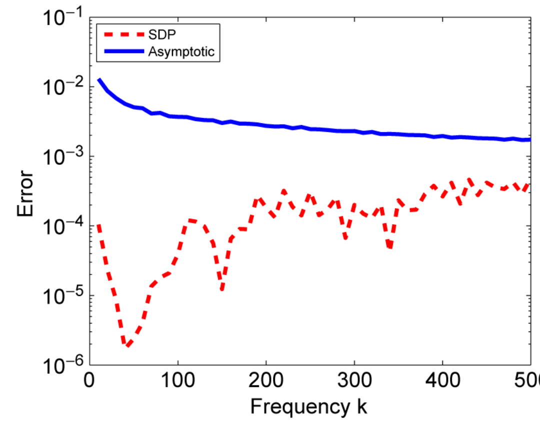

Fig. 13. Red line: The relative error of the bistatic scattered electric field $\mathbf{E}_s(\mathbf{r})$ results [see (4)] produced by using the NSDP method relative to the brute force method on the parabolic patch. Blue line: The relative error of the bistatic scattered electric field $\mathbf{E}_s(\mathbf{r})$ results [see (4)] produced by using the traditional asymptotic expansion method [17] relative to the brute force method on the parabolic patch.

B. Comparisons of the Similarities and Differences Between the Numerical Steepest Descent Path Method and the Asymptotic Expansion Method

The similarities between the numerical steepest descent path method and the asymptotic expansion method in [17] are, first, the amplitude and phase terms in the PO integrands are approximated as polynomials, and quadratic variations of the phase terms are considered in both works. Second, triangular discretization patches are used. Thirdly, surface PO integral is reduced to several line integrals. Finally, the computational cost is wave frequency independent.

The differences between both works are, first, the work in [17], [18] is done by using the divergence theorem to reduce the PO surface integral as several line integrals. Their line integrals are expressed in terms of special generalized Fresnel functions, and the transition functions. The numerical steepest descent path (NSDP) algorithm in this paper is proposed by using the contour deformation in the complex plane, and the resultant PO line integrals are expressed in terms of exponentially decay integrand defined on the corresponding NSDPs. Second, in this work, both the amplitude and the phase terms in the PO integrand are second order polynomials. In the recent work [18], the amplitude is assumed to be linear and the phase term is quadratic. Finally, the NSDP algorithm for the PO integral is done exactly with only numerical approximation. And the asymptotic expansion in [18] is used for general type PO integrand.

To show the strength of the NSDP method for calculating $\mathbf{E}_s(\mathbf{r})$ on the parabolic patch, Figs. 12, 13 present the comparison of relative errors between the NSDP and asymptotic expansion [17] methods relative to the brute force method. From these two figures, it can be seen that the NSDP method can significantly improve the $\mathbf{E}_s(\mathbf{r})$ accuracy by around two digits (10^{-2}) when the working frequency k is not extremely large, including both the monostatic and bistatic cases. Numerical tests also show that the comparison relative errors by these two methods rely on the parameters of the incident wave and observation point vectors.

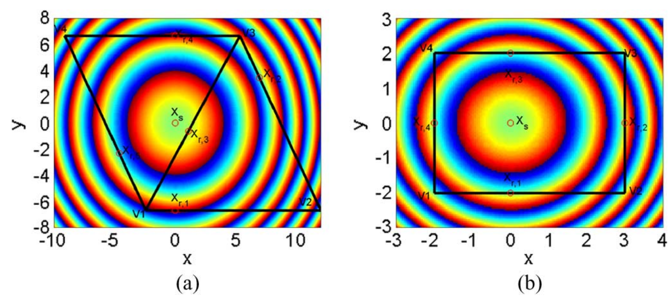

Fig. 14. (a): The $x-y$ quadrilateral domain $\mathbf{V}_1\mathbf{V}_2\mathbf{V}_3\mathbf{V}_4$ of the parabolic PEC patch shown in Fig. 4. (b): The $x-y$ affine transformed quadrilateral domain in Fig. 14(a).

C. The Rectangular Domain Example

The second example is the PO surface integral $\tilde{I}$ defined on the rectangular domain. After the affine transformation of the quadrilateral domain $\mathbf{V}_1\mathbf{V}_2\mathbf{V}_3\mathbf{V}_4$ as shown in Fig. 14(a), a rectangular domain in the $x-y$ domain is presented in Fig. 14(b). The canonical form PO integral $\tilde{I}$ given in (11) has the closed-form formula in terms of the special complementary error function (see Appendix B).

The parameters are the same as those in the monostatic case of Example 1 except that we consider the rectangular domain in Fig. 14(b). In Fig. 15, we show the RCS results of the PO scattered electric field $\mathbf{E}_s(\mathbf{r})$ by using the NSDP method and the closed-form formula (49) in Appendix B. The results achieved by the NSDP method agree well with those by the closed-form formula, and the computational efforts are frequency-independent.

Physically, the contributions to the PO integral $\tilde{I}$ expressed in (34) can be classified into those from the stationary phase point, the boundary resonance points and boundary vertex points. In [36], the stationary phase point, resonance and vertex points contributions by the NSDP method are exactly extracted. Fig. 16 presents the comparison of the total vertex and resonance point contributions for the PO integral $\tilde{I}$ by using the NSDP method

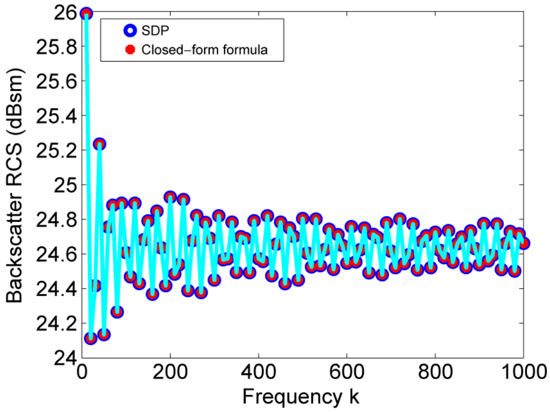

Fig. 15. Comparisons of the RCS (dBsm unit) values of the PO scattered electric field (7) by using the NSDP method and the closed-form formula (49).

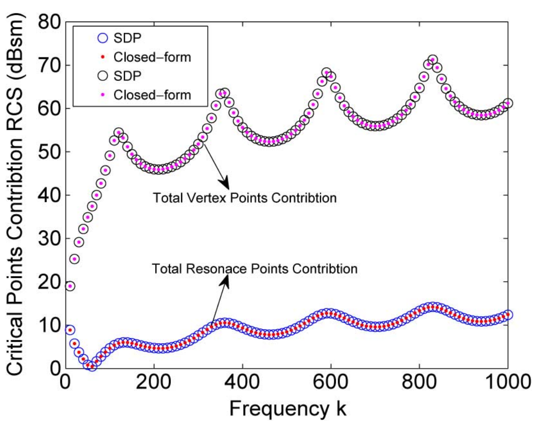

Fig. 16. Comparisons of the total vertex and resonance points contributions for the PO scattered electric field (7) by using the NSDP method and the closed-form formula.

and the asymptotic expansion approach in [17]. It can be observed that the critical point contribution results produced by both methods agree well with each other when the frequency k is large enough.

VII. Conclusion

In this work, we propose the NSDP method to calculate the highly oscillatory PO integral on the parabolic patch, including both monostatic and bistatic cases. The PO scattered field is expressed as the highly oscillatory surface integrals defined on the assembled triangular patches. Quadratic functions are used to approximate the phase and amplitude terms of the PO integrand. After the affine transformation, the PO integral on the triangular patch is simplified to its canonical form. By invoking the NSDP method, the canonical form PO integral on the assembled triangular patches is expressed based on the NSDPs. Numerical examples illustrate that the proposed NSDP method for the surface PO integral is frequency-independent and error-controllable. Furthermore, compared with the asymptotic expansion approach, the proposed NSDP method can improve the electric scattered field accuracy by around two digits when the working wave frequencies are not large enough.

Appendix A
Canonical Forms of the Quadratic PO Integrals

We notice that $\tilde{v}_n(x,y)$ in (12) can be expressed in terms of the matrix notation as

$$\begin{aligned}\tilde{v}_n(x,y) &= [x \quad y]\cdot \mathbf{W}_n \cdot \begin{bmatrix} x \\ y\end{bmatrix} + \tilde{\beta}_{n,2}x + \tilde{\beta}_{n,3}y + \tilde{\beta}_{n,1} \\ &= [x-\tilde{a}_n \quad y-\tilde{c}_n]\cdot \mathbf{W}_n \cdot \begin{bmatrix} x-\tilde{a}_n \\ y-\tilde{c}_n\end{bmatrix} + \tilde{G}_n \end{aligned} \tag{40}$$

where the symmetric matrix $\mathbf{W}_n$ has the form

$$\mathbf{W}_n = \begin{bmatrix} \tilde{\beta}_{n,4} & \frac{\tilde{\beta}_{n,6}}{2} \\ \frac{\tilde{\beta}_{n,6}}{2} & \tilde{\beta}_{n,5}\end{bmatrix}. \tag{41}$$

We consider the case that $\mathbf{W}_n$ is nondegenerate. In (40), $\tilde{G}_n$ is a constant, then the coefficients $\tilde{a}_n$ and $\tilde{c}_n$ can be uniquely determined by the relationships

$$\begin{aligned}\tilde{\beta}_{n,2} + 2\tilde{\beta}_{n,4}\tilde{a}_n + \tilde{\beta}_{n,6}\tilde{c}_n &= 0 \\ \tilde{\beta}_{n,3} + 2\tilde{\beta}_{n,5}\tilde{c}_n + \tilde{\beta}_{n,6}\tilde{a}_n &= 0.\end{aligned}$$

More specifically

$$\begin{bmatrix}\tilde{a}_n \\ \tilde{c}_n\end{bmatrix} = (2\mathbf{W}_n)^{-1}\cdot \begin{bmatrix} -\tilde{\beta}_{n,2} \\ -\tilde{\beta}_{n,3}\end{bmatrix}. \tag{42}$$

The coefficient $\tilde{G}_n$ in (40) is

$$\tilde{G}_n = -\left(\tilde{\beta}_{n,4}\tilde{a}_n^2 + \tilde{\beta}_{n,5}\tilde{c}_n^2 + \tilde{\beta}_{n,6}\tilde{a}_n\tilde{c}_n - \tilde{\beta}_{n,1}\right). \tag{43}$$

Since the matrix $\mathbf{W}_n$ is nondegenerate and symmetric, we can always find the invertible congruent transformation matrix $\mathbf{Q}_n$, such that

$$\mathbf{Q}_n^T \cdot \mathbf{W}_n \cdot \mathbf{Q}_n = \mathbf{D}_n = \begin{bmatrix}\chi_{n,1} & \\ & \chi_{n,2}\end{bmatrix} \tag{44}$$

where

$$\mathbf{Q}_n = \begin{bmatrix} q_{n,11} & q_{n,12} \\ q_{n,21} & q_{n,22}\end{bmatrix} = \begin{bmatrix} \sqrt{|\tilde{\beta}_{n,4}|} & -\dfrac{\tilde{\beta}_{n,6}}{2\sqrt{|\tilde{\beta}_{n,4}|}\sqrt{\left|\tilde{\beta}_{n,5}-\tilde{\beta}_{n,4}^{-1}\left(\frac{\tilde{\beta}_{n,6}}{2}\right)^2\right|}} \\ 0 & \dfrac{1}{\sqrt{\left|\tilde{\beta}_{n,5}-\tilde{\beta}_{n,4}^{-1}\left(\frac{\tilde{\beta}_{n,6}}{2}\right)^2\right|}}\end{bmatrix} \tag{45}$$

and $\chi_{n,j} = 1$ or -1, for $j = 1$ or 2. Combining (40)–(44), and using the coordinate transformation, we have

$$\begin{bmatrix} x' \\ y'\end{bmatrix} = \mathbf{Q}_n^{-1}\cdot\begin{bmatrix} x-\tilde{a}_n \\ y-\tilde{c}_n\end{bmatrix}. \tag{46}$$

The quadratic phase function $\tilde{v}_n(x,y)$ in (12) can be simplified to its canonical form:

$$\tilde{v}_n(x',y') = \chi_{n,1}(x')^2 + \chi_{n,2}(y')^2, \tag{47}$$

with $\chi_{n,j} = 1$ or -1, for $j = 1$ or 2. The matrix $\mathbf{Q}_n^{-1}$ in (46) has the formula

$$\mathbf{Q}_n^{-1} = \begin{bmatrix} q_{n,11}^{-1} & q_{n,22}^{-1}\left(q_{n,12} - q_{n,11}^{-1}q_{n,12}\right) \\ 0 & q_{n,22}^{-1}\end{bmatrix}. \tag{48}$$

Notice that the coordinate transform in (46) is an affine transformation. Then, it will always map the triangle $\triangle_n$ to another triangle $\triangle'_n$. In this manner, in Section II, each summation integral term in (11) can be written as (14).

APPENDIX B
THE CLOSED-FORM FORMULA OF THE PO INTEGRAL $\tilde{I}$ ON THE RECTANGULAR DOMAIN

In Fig. 14(b), we denote the x and y values of the four corners on the rectangular domain $\mathbf{V}_1\mathbf{V}_2\mathbf{V}_3\mathbf{V}_4$ as $\mathbf{V}_m(1)$ and $\mathbf{V}_m(2)$, $m = 1, 2, 3, 4$. Then, the PO integral $\tilde{I}$ on the rectangular domain has the closed-form formula

$$\begin{aligned}\tilde{I} &= \int_{\mathbf{V}_1(1)}^{\mathbf{V}_2(1)} \int_{\mathbf{V}_1(2)}^{\mathbf{V}_4(2)} p(x,y) e^{ik(x^2+y^2)} dydx, \\ &= \int_{\mathbf{V}_1(1)}^{\mathbf{V}_2(1)} e^{ikx^2} \left[T\left(\mathbf{V}_4(2), x\right) - T\left(\mathbf{V}_1(2), x\right)\right] dx \\ &= S(\mathbf{V}_3) - S(\mathbf{V}_2) - \left[S(\mathbf{V}_4) - S(\mathbf{V}_1)\right] \end{aligned} \tag{49}$$

where

$$\begin{aligned} T\left(\mathbf{V}_l(2), x\right) &= \frac{\alpha_3 + \alpha_6 x + \alpha_5 \mathbf{V}_l(2)}{2ik} e^{ik\mathbf{V}_l(2)^2} \\ &- \frac{\sqrt{\pi}}{2\sqrt{-ik}} \left(\alpha_1 + \alpha_2 x + \alpha_4 x^2 - \frac{\alpha_5}{2ik}\right) \operatorname{erfc}\left(\sqrt{-ik}\mathbf{V}_l(2)\right) \end{aligned}$$

$l = 1, 4$, and

$$\begin{aligned} S(\mathbf{V}_m) &= \left[Z_1\left(\mathbf{V}_m(2)\right) + Z_2\left(\mathbf{V}_m(1)\right)\right] \\ &\quad \operatorname{erfc}\left(\sqrt{-ik}\mathbf{V}_m(1)\right) + Z_3\left(\mathbf{V}_m(1)\right) e^{ik\mathbf{V}_m(1)^2}, \\ Z_1\left(\mathbf{V}_m(2)\right) &= -\frac{\pi}{4ik}\alpha_1 \operatorname{erfc}\left(\sqrt{-ik}\mathbf{V}_m(2)\right) \\ &\quad - \frac{\pi}{8k^2}\left(\alpha_4 + \alpha_5\right) \operatorname{erfc}\left(\sqrt{-ik}\mathbf{V}_m(2)\right) \\ &\quad - \frac{\sqrt{\pi}}{4ik\sqrt{-ik}} \alpha_3 e^{ik\mathbf{V}_m(2)^2} \\ &\quad - \frac{\sqrt{\pi}}{4ik\sqrt{-ik}} \alpha_5 \mathbf{V}_m(2) e^{ik\mathbf{V}_m(2)^2} \\ Z_2\left(\mathbf{V}_m(1)\right) &= -\frac{\sqrt{\pi}}{4ik\sqrt{-ik}}\alpha_2 - \frac{\sqrt{\pi}\mathbf{V}_m(1)}{4ik\sqrt{-ik}}\alpha_4 \\ Z_3\left(\mathbf{V}_m(1)\right) &= -\frac{1}{4k^2}\alpha_6 e^{ik\mathbf{V}_m(1)^2}, m = 1,2,3,4. \end{aligned} \tag{50}$$

REFERENCES

[1] O. M. Conde, J. Pérez, and M. F. Cátedra, "Stationary phase method application for the analysis of radiation of complex 3-D conducting structures," *IEEE Trans. Antennas Propag.*, vol. 49, no. 5, pp. 724–731, May 2001.
[2] R. H. Harrington, *Field Computation by Moment Method*. Piscataway, NJ, USA: IEEE Press, 1993.
[3] W. C. Chew, *Waves and Fields in Inhomogeneous Media*. Piscataway, NJ, USA: IEEE Press, 1995.
[4] J. A. Kong, *Electromagnetic Wave Theory*. New York, NY, USA: Wiley-Interscience, 1990.
[5] C. A. Balanis, *Advanced Engineering Electromagnetics*. New York: Wiley, 1989.
[6] E. F. Knott, J. F. Shaeffer, and M. T. Tuley, *Radar Cross Section*. Norwood, MA, USA: Artech House, 1993.
[7] H. M. Macdonald, "The effect produced by an obstacle on a train of electric waves," *Phil. Trans. Royal Soc. London, Series A, Math. Phys. Sci.*, vol. 212, pp. 299–337, 1913.
[8] P. Y. Ufimtsev, "New insight into the classical Macdonald physical optics approximation," *IEEE Antennas Propag. Mag.*, vol. 50, pp. 11–20, Jun. 2008.
[9] P. Y. Ufimtsev, *Backscatter*. Hoboken, NJ, USA: Wiley, 2005.
[10] S. W. Lee and R. Mittra, "Fourier transform of a polygonal shape function and its application in electromagnetics," *IEEE Trans. Antennas Propag.*, vol. 31, no. 1, pp. 99–103, Jan. 1983.
[11] G. D. Crabtree, "A numerical quadrature technique for physical optics scattering analysis," *IEEE Trans. Magn.*, vol. 27, no. 9, pp. 4291–4294, Sep. 1991.
[12] D. Bolukbas and A. A. Ergin, "A radon transform interpretation of the physical optics integral," *Microw. Opt. Tech. Lett.*, vol. 44, pp. 284–288, Feb. 2005.
[13] R. J. Burkholder and T. H. Lee, "Adaptive sampling for fast physical optics numerical integration," *IEEE Trans. Antennas Propag.*, vol. 53, no. 5, pp. 1843–1845, May 2005.
[14] F. Obelleiro-Basteiro, J. L. Rodriguez, and R. J. Burkholder, "An iterative physical optics approach for analyzing the electromagnetic scattering by large open-ended cavities," *IEEE Trans. Antennas Propag.*, vol. 43, no. 4, pp. 356–361, Apr. 1995.
[15] M. F. Cátedra, C. Delgado, S. Luceri, O. G. Blanco, and F. S. Adana, "Physical optics analysis of multiple interactions in large scatters using current modes," *IEEE Trans. Antennas Propag.*, vol. 54, no. 3, pp. 985–994, Mar. 2006.
[16] M. F. Cátedra, C. Delgado, and I. G. Diego, "New physical optics approach for an efficient treatment of multiple bounces in curved bodies defined by an impedance boundary condition," *IEEE Trans. Antennas Propag.*, vol. 56, no. 3, pp. 728–736, Mar. 2008.
[17] G. Carluccio, M. Albani, and P. H. Pathak, "Uniform asymptotic evaluation of surface integrals with polygonal integration domains in terms of UTD transition functions," *IEEE Trans. Antennas Propag.*, vol. 58, no. 4, pp. 1155–1163, Apr. 2010.
[18] G. Carluccio and M. Albani, "Efficient adaptive numerical integration algorithms for the evaluation of surface radiation integrals in the high-frequency regime," *Radio Sci.*, vol. 46, Jun. 2011, RS0E04.
[19] M. Albani, "Boundary diffracted wave and incremental geometrical optics: A numerically efficient and physically appealing line-integral representation of radiation integrals. Aperture scalar case," *IEEE Trans. Antennas Propag.*, vol. 59, no. 2, pp. 586–594, Feb. 2011.
[20] G. Carluccio, F. Puggelli, and M. Albani, "Algorithm for the computation of the generalized Fresnel integral," *IEEE Trans. Antennas Propag.*, vol. 59, no. 10, pp. 3943–3947, Oct. 2011.
[21] F. Puggelli, G. Carluccio, and M. Albani, "An efficient algorithm for the computation of the UTD T transition function," *IEEE Trans. Antennas Propag.*, vol. 60, no. 5, pp. 2380–2387, May 2012.
[22] A. Iserles and S. P. Nøsett, "Quadrature methods for multivariate highly oscillatory integrals using derivatives," *Math. Comp.*, vol. 75, pp. 1233–1258, Jul. 2006.
[23] A. Iserles and S. P. Nøsett, "From high oscillation to rapid approximation III: Multivariate expansions," *IMA J. Num. Anal.*, vol. 29, pp. 882–916, 2009.
[24] A. Iserles and D. Levin, "Asymptotic expansion and quadrature of composite highly oscillatory integrals," *Math. Comp.*, vol. 80, pp. 279–296, Jan. 2011.
[25] D. Huybrechs and S. Vandewalle, "The construction of cubature rules for multivariate highly oscillatory integrals," *Math. Comp.*, vol. 76, pp. 1955–1980, Oct. 2007.
[26] D. Huybrechs and S. Vandewalle, "A sparse discretisation for integral equation formulations of high frequency scattering problems," *SIAM J. Sci. Comput.*, vol. 29, pp. 2305–2328, 2007.
[27] A. Asheim and D. Huybrechs, "Asymptotic analysis of numerical steepest descent with path approximations," *Found. Comput. Math.*, vol. 10, pp. 647–671, 2010.
[28] W. B. Gordon, "Far-field approximations to the Kirchhoff-Helmholtz representation of scattered fields," *IEEE Trans. Antennas Propag.*, vol. 23, no. 7, pp. 590–592, Jul. 1975.
[29] W. B. Gordon, "High-frequency approximations to the physical optics scattering integral," *IEEE Trans. Antennas Propag.*, vol. 42, pp. 427–432, Mar. 1994.
[30] L. Infante and M. Stefano, "Near-field line-integral representation of the Kirchhoff-type aperture radiation for parabolic reflector," *IEEE Antennas Wireless Propag. Lett.*, vol. 2, pp. 273–276, 2003.
[31] C. Delgado, J. M. Gómez, and M. F. Cátedra, "Analytical field calculation involving current modes and quadratic phase expressions," *IEEE Trans. Antennas Propag.*, vol. 55, no. 1, pp. 233–240, Jan. 2007.

[32] F. Vico, M. Ferrando, and A. Valero, "A new fast physical optics for smooth surfaces by means of a numerical theory of diffraction," *IEEE Trans. Antennas Propag.*, vol. 58, pp. 773–789, Mar. 2010.
[33] S. Josef and B. Roland, *Introduction to Numerical Analysis*. Berlin, Germany: Springer-Verlag, 1980.
[34] M. Abramowitz and I. A. Stegun, *Handbook of Mathematical Functions*. Norwood, MA, USA: Dover, 1972.
[35] C. P. Davis and W. C. Chew, "Frequency-independent scattering from a flat strip with TE_z-polarized fields," *IEEE Trans. Antennas Propag.*, vol. 56, no. 4, pp. 1008–1016, Apr. 2008.
[36] Y. M. Wu, L. J. Jiang, and W. C. Chew, "An efficient method for computing highly oscillatory physical optics integral," *Progr. Electromagn. Res. PIER*, vol. 127, pp. 211–257, 2012.
[37] Y. M. Wu, L. J. Jiang, and W. C. Chew, "An efficient method for highly oscillatory physical optics integrals," in *Proc. 2012 IEEE Antennas Propag. Int. Symp.*, Chicago, IL, Jul. 8–14, .

Yu Mao Wu received the Ph.D. degree in computational mathematics from the University of Science and Technology of China (USTC), Hefei, China, in 2010.

He is currently a Postdoctoral Research Fellow with the Department of Electrical and Electronic Engineering, the University of Hong Kong (HKU), Hong Kong. His research interests include high frequency wave propagation, inverse scattering problems in electromagnetics, integral equation methods and fast algorithms in computational electromagnetics, and numerical methods in periodic structures. He has authored or coauthored more than 10 papers in refereed journals and conference proceedings.

Dr. Wu was the recipient of the Best Student Paper Award presented at the International Conference on Applied Mathematics: Modeling, Analysis, and Computation in June 2008, in Hong Kong.

Li Jun Jiang (S'01–M'04–SM'13) received the B.S. degree in electrical engineering from the Beijing University of Aeronautics and Astronautics, Beijing, China, in 1993, the M.S. degree from Tsinghua University, Tsinghua, China, in 1996, and the Ph.D. degree from the University of Illinois at Urbana-Champaign, Urbana, IL, USA, in 2004.

From 1996 to 1999, he was an Application Engineer with the Hewlett-Packard Company. Since 2004, he has been a Postdoctoral Researcher, a Research Staff Member, and a Senior Engineer at the IBM T.J. Watson Research Center. Since the end of 2009, he has been an Associate Professor with the Department of Electrical and Electronic Engineering at the University of Hong Kong, Hong Kong. His research interests include electromagnetics, EMC/EMI, antennas, multidisciplinary EDA solutions, RF and microwave technologies, and high performance computing (HPC), etc.

Dr. Jiang received the HP STAR Award, in 1998. In 2003, he received the IEEE MTT Graduate Fellowship Award, and in 2004, he received the Y.T. Lo Outstanding Research Award. In 2008, he received the IBM Research Technical Achievement Award. He was the Semiconductor Research Cooperation (SRC) Industrial Liaison for several academic projects. Since 2009, he has been the SRC Packaging High Frequency Topic TT Chair. He has served as the Technical Committee Member for IEEE EDAPS since 2010, the Scientific Committee Member of 2010 IEEE SMEE, and the Guest Associate Editor of the IEEE PROCEEDINGS since 2011. He was the Scientific Consultant of HK ASTRI in 2010. He is a Member of the IEEE AP-S, IEEE MTT-S, ACES, Sigma Xi, and Chinese CEM Society. He has been serving as the reviewer of many primary professional EM related journals, and special sessions organizer and session chairs of many international conferences.

Wei E. I. Sha (M'09) received the B.S. and Ph.D. degrees in electronic engineering from Anhui University, Hefei, China, in 2003 and 2008, respectively.

From July 2008 to May 2012, he was a Postdoctoral Research Fellow with the Department of Electrical and Electronic Engineering at the University of Hong Kong, Hong Kong, where he is now a Research Assistant Professor. He has authored or coauthored about 40 international technical Journals, contributed to two book chapters at Springer and InTech Publishers, and one book on wavelet theory and applications. His research interests include applied and computational electromagnetics, nano-optics and quantum-optics, solar cells and optoelectronics, multiphysics modeling and understanding, etc.

Dr. Sha is a Member of Antennas and Propagation Society and Photonics Society. He is also a Member of OSA. He served as a Reviewer of IEEE, OSA, and AIP Journals. In 2007, he was awarded the first prize for the Outstanding Paper at The Fourth National Postgraduates Mathematical Contest in Modeling of China. At the same year, he received the China Adolescents Science and Technology Innovation Award at the Great Hall of the People.

Weng Cho Chew (S'79–M'80–SM'86–F'93) received the B.S. degree in 1976, the M.S. and Engineer's degrees in 1978, and the Ph.D. degree in 1980, all in electrical engineering, from the Massachusetts Institute of Technology, Cambridge, MA, USA.

He served as the Dean of Engineering at The University of Hong Kong, Hong Kong from 2008 to 2011. He was a Professor and the Director of the Center for Computational Electromagnetics and the Electromagnetics Laboratory, the University of Illinois at Urbana-Champaign, Urbana, IL, USA. Before joining the University of Illinois at Urbana-Champaign, he was the Department Manager and a Program Leader at Schlumberger-Doll Research, Cambridge, MA, USA. He is the Originator of several fast algorithms for solving electromagnetics scattering and inverse problems. He has led a research group that has developed parallel codes to solve dense matrix systems with tens of millions of unknowns for the first time for integral equations of scattering. He has authored a book entitled *Waves and Fields in Inhomogeneous Media* (New York: IEEE Press, 1999), coauthored two books entitled *Fast and Efficient Methods in Computational Electromagnetics* (Boston, MA: Artech House, 2001) and *Integral Equation Methods for Electromagnetic and Elastic Waves* (1st ed. San Rafael, CA: Morgan & Claypool Publishers, 2007), authored or coauthored more than 300 journal publications, more than 400 conference publications, and more than ten book chapters. His research interests include the areas of waves in inhomogeneous media for various sensing applications, integrated circuits, microstrip antenna applications, and fast algorithms for solving wave scattering and radiation problems.

Dr. Chew served on the IEEE Adcom for Antennas and Propagation Society as well as on the Geoscience and Remote Sensing Society. He has been active with various journals and societies. He is a Fellow of the Optical Society of America, Institute of Physics, Electromagnetics Academy, Hong Kong Institute of Engineers, and was the National Science Foundation Presidential Young Investigator. He received the Schelkunoff Best Paper Award for Antennas and Propagation (AP) Transaction, the IEEE Graduate Teaching Award, the UIUC Campus Wide Teaching Award, and the IBM Faculty Awards. He was a Founder Professor of the College of Engineering, and previously, the First Y. T. Lo Endowed Chair Professor in the Department of Electrical and Computer Engineering, the University of Illinois at Urbana-Champaign. From 2005 to 2007, he served as an IEEE Distinguished Lecturer. He served as the Cheng Tsang Man Visiting Professor at Nanyang Technological University, Singapore, in 2006. In 2002, the Institute for Science Information Citation elected him to the category of most highly cited authors (top 0.01%). In 2008, he was elected by the IEEE AP Society to receive the Chen-To Tai Distinguished Educator Award. He is currently the Editor-in-Chief of the *Journal of Electromagnetic Waves and Applications/Progress in Electromagnetic Research Journal*, and on the Board of Directors of Applied Science Technology Research Institute, Hong Kong. He has been recently elected to the National Academy of Engineering.